Electronic Supplementary Material (ESI) for Journal of Materials Chemistry A.

Efficient Water Oxidation under Visible Light by Tuning Surface Defects on Ceria Nanorods

Kun Zhao,[a,b] Jian Qi,[c] Huajie Yin,[b] Zumin Wang,[a] Shenlong Zhao,[b] Xiang Ma,[b] Jiawei Wan,[b] Lin Chang,[b] Yan Gao,*[b] Ranbo Yu*[a] and Zhiyong Tang*[b]

[a] *Department of Physical Chemistry, School of Metallurgical and Ecological Engineering, University of Science and Technology Beijing, Beijing 100083, P. R. China. E-mail: ranboyu@ustb.edu.cn*

[b] *Key Laboratory of Nanosystem and Hierarchical Fabrication, National Center for Nanoscience and Technology, Beijing 100190, P. R. China. Fax: (+86)10-62656765. E-mail: zytang@nanoctr.cn, gaoyan@nanoctr.cn*

[c] *National Key Laboratory of Biochemical engineering, Institute of Process Engineering, Chinese Academy of Sciences, Beijing 100190, P. R. China.*

Experimental Section

Reagents: All the reagents including CeO_2, $CeCl_3 \cdot 7H_2O$, ethanol, ammonia solution (25%) and $AgNO_3$ were analytical grade and bought from Beijing Chemical Reagent Factory. They were used in the experiment without further purification. Ultrapure water (Millipore Milli-Q grade) with a resistivity of 18.2 MΩ.cm (25^{o}C) was used in all the experiments.

Synthesis of CeO_2 nanorods (NRs): In a typical procedure, 1.2 g $CeCl_3 \cdot 7H_2O$ was dissolved in 15 mL pure water to form a clear solution **A**. Then, 15 mL ethanol was added into solution **A** to form the clear solution **B**, and stirred for 10 min. Subsequently, the aqueous ammonia solution was added drop by drop into the solution **B** under vigorous stirring to produce a grey colloidal solution **C** with pH value of about 9.3-9.5. Afterward, the colloidal solution **C** was transferred and sealed in a Teflon-sealed stainless steel autoclave (volume = 50 mL). The autoclave was kept at 140^{o}C for 56 h. When the reaction was completed, a rinsing process including three cycles of alternative washing with pure water and ethanol was carried out before drying in an oven at room temperature for 24 h. Finally, as-synthesized solid powder was calcined in a tube furnace under Ar-H_2, Ar or Air atmosphere at different temperature of 100^{o}C, 300^{o}C, 500^{o}C and 800^{o}C, respectively. The rate of temperature increase was controlled to be 1^{o}C / min, and the calcination duration was set to 180 min.

Photocatalytic test: The photocatalytic experiments were carried out in a 300 mL pyrex reactor under photoirradiation coupled an online gas chromatograph (GC, TianMei company, GC-7900, Ar as the carrier gas) equipped with a thermal conductivity detector. The photocatalyst (50 mg) was firstly dispersed in a 75 mL 0.01 M $AgNO_3$ aqueous solution and then ultrasonicated for 10 min. Subsequently, the suspension was transferred into the reactor and then purged by a vacuum pump before photo-irradiation in order to remove the dissolved air. A 300 W xenon lamp with a cutoff filter ($\lambda \geq 420$ nm) (Beijing Perfect Light Company) was used to irradiate the suspension, and the O_2 evolution was determined quantitatively by GC. The optical density of the light source with a 420 cutoff filter was about 280.16 mw cm^2, which was measured by by a Thorlab optical

power meter. The length was about 15 cm between the reaction liquid level and light source. The cooling water was set at 7.5°C.

Durability of photocatalysts: The photocatalytic durability experiments were also performed in a 300 mL pyrex reactor under photoirradiation coupled online with a GC equipped with a thermal conductivity detector. The photocatalyst (50 mg) was firstly dispersed in a 75 mL 0.01 M $AgNO_3$ aqueous solution and then untrasonicated for 10 min. Subsequently, the suspension was transferred into the reactor and then purged by a vacuum pump before photo-irradiation in order to remove the dissolved air. A 300 W xenon lamp with cutoff filter ($\lambda \geq 420$ nm) (Beijing Perfect Light Company) was used to irradiate the suspension and the O_2 evolution were determined quantitatively by GC. Every cycle was carried out for 2 h, and at the beginning of the second and third cycles 0.128 g $AgNO_3$ and 8 mL H_2O were added into the reactor. During the interruption of each cycle, the system was vacuumed for 5 min.

Photocatalyst band gap calculation: The following equation proposed by Tauc, Davis, and Mott was used.

$(h\nu\alpha)^{1/n} = A(h\nu - E_g)$ .....equation (1)

Where h was Planck's constant, ν represented frequency of vibration, α stood for absorption coefficient, E_g was band gap, A represented proportional constant.

The value of the exponent n denoted the nature of the sample transition.

For direct allowed transition$\cdots\cdots n = 1/2$

For direct forbidden transition $\cdots\cdots n = 3/2$

For indirect allowed transition $\cdots\cdots n = 2$

For indirect forbidden transition $\cdots\cdots n = 3$

Since CeO_2 belonged to the direct allowed sample transition, $n = 1/2$ was used in our experiment.

The acquired diffuse reflectance spectrum was converted to Kubelka-Munk function. Thus, the

vertical axis was converted to quantity F(R∞), which was proportional to the absorption coefficient. The α in the Tauc equation was substituted with F(R∞). Thus, in the experiment, the expression became:

$(h\nu F(R\infty))^2 = A(h\nu - E_g)$..... equation (2)

Using the Kubelka-Munk function, the $(h\nu F(R\infty))^2$ was plotted against $h\nu$. The curve, plotting of the value of $(h\nu - (h\nu F(R\infty))^2)$ on the horizontal axis $h\nu$ and vertical axis $(h\nu F(R\infty))^2$, was drawn. Here, the unit for $h\nu$ was eV (electron volt), and its relationship to the wavelength λ (nm) became

$h\nu = 1239.7/\lambda$..... equation (3)

A line was drawn tangent to the point of inflection on the curve, and the $h\nu$ value at the point of intersection of the tangent line and the horizontal axis was the value of band gap E_g (Figure 5c).

Characterization: Scanning electron microscopy (SEM) was performed on a Hitachi S-4800 electron microscope. Transmission electron microscopy (TEM) was carried out on FEI Tecnai G^2 F20 electron microscope operated at 200 kV with the software package for automated electron tomography. Powder X-ray diffraction (XRD) patterns were recorded on a Rigaku Corporation X-ray power diffraction using Cu Kα radiation (λ=1.54056 Å). Fourier-transform infrared (FTIR) spectra were acquired with PE2000 (USA). XPS spectra were performed by an ESCALAB 250 Xi XPS system of Thermo Scientific, where the analysis chamber was 1.5×10^{-9} mbar and the X-ray spot was set to 500 μm. The BET (Brunauer-Emmett-Teller) surface area, pore volume and pore size of catalysts were measured using a Quadrasorb SI-MP instrument. Electron paramagnetic resonance (EPR) spectrum was acquired by JES-FA-200 (JEOL). (Test condition: sample weight, 100mg; temperature, 103 K) Ultraviolet photoelectrons spectroscopy (UPS) was carried out using a UPS system (Thermo Scientific, ESCLAB 250Xi, USA). Prior to each measurement, the sample was heated to 100°C and kept at this temperature for 2 h. UV-Vis diffuse reflection absorption spectra (UV-Vis/DRS) of the samples were recorded by an UV-Vis spectrometer (Lambda 950, PE, USA) equipped with an integrating sphere accessory in the diffuse reflectance mode (R) and

$BaSO_4$ as reference material. The sample weight was about 10 mg, which was uniformly distributed in an area of about 1.5 cm^2 in size.

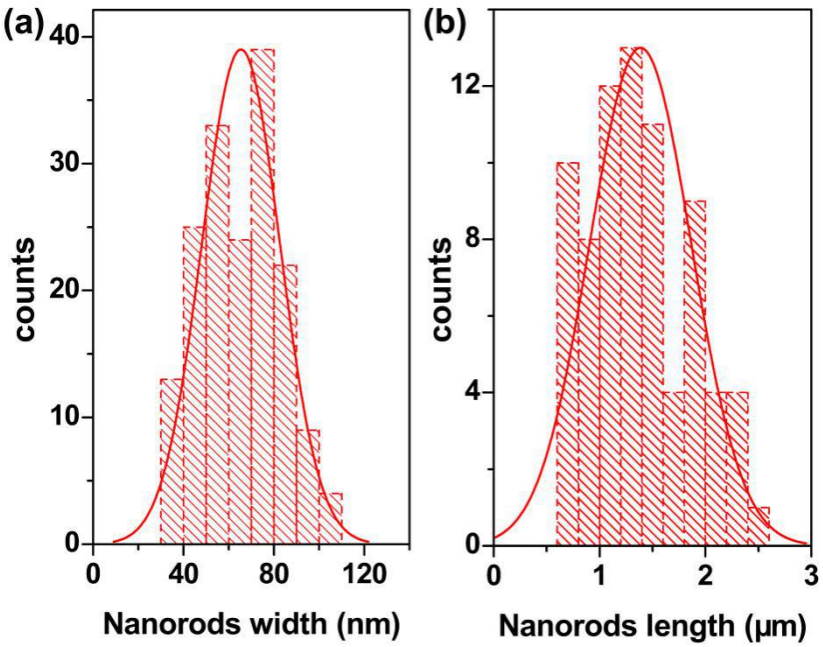

Fig. S1 Statistic histogram of width (a) and length (b) distribution of Ce-based NRs.

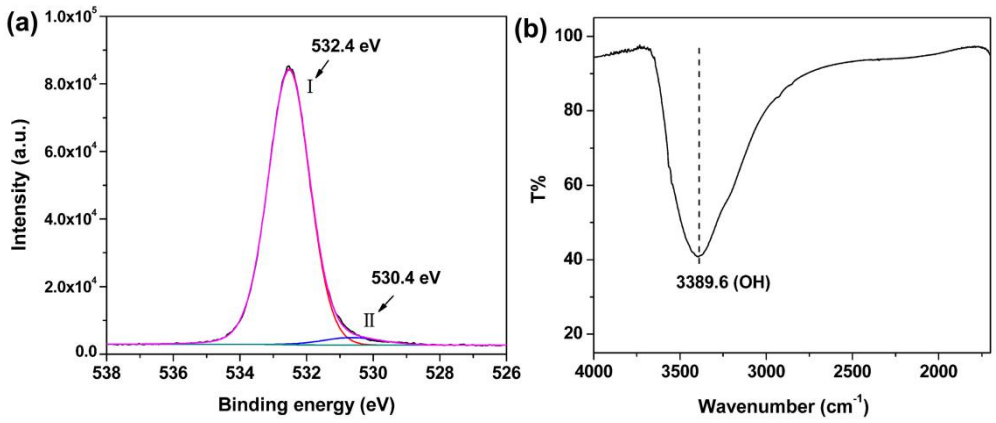

Fig. S2 (a) XPS O1s and (b) FTIR spectra of Ce-based NRs**.**

In **Fig. S2a**, the peak I at 532.4 eV is assigned to the hydroxyl groups ($Ce(OH)_3$ and adsorbed water gas) that are called as absorbed oxygen. Another small peak II located at 530.4 eV is the active oxygen from crystallized Ce_2O_3. There is no observable lattice oxygen in as-synthesized Ce-based NRs. In **Fig. S2b**, the peak located at 3389.6 cm^{-1} is also attributed to hydroxyl groups.

Table S1 Heat-treatment parameters including temperature, time and atmospheres for different catalysts.

Temp. / Time / Atmos.	100°C	300°C	500°C	800°C
Ar-H_2	3 h	3 h	3 h	3 h
Ar	3 h	3 h	3 h	3 h
Air	3 h	3 h	3 h	3 h

As-synthesized Ce-based composites were heat treated under different atmosphere (Ar mixed with H_2 (10% in volume), Ar and air) at 100°C, 300°C, 500°C or 800°C, respectively. Consequently, photocatalysts were obtained and named as Ar-H_2-100, Ar-H_2-300, Ar-H_2-500, Ar-H_2-800, Ar-100, Ar-300, Ar-500, Ar-800, Air-100, Air-300, Air-500 and Air-800, respectively. All the samples were calcined for 3 h.

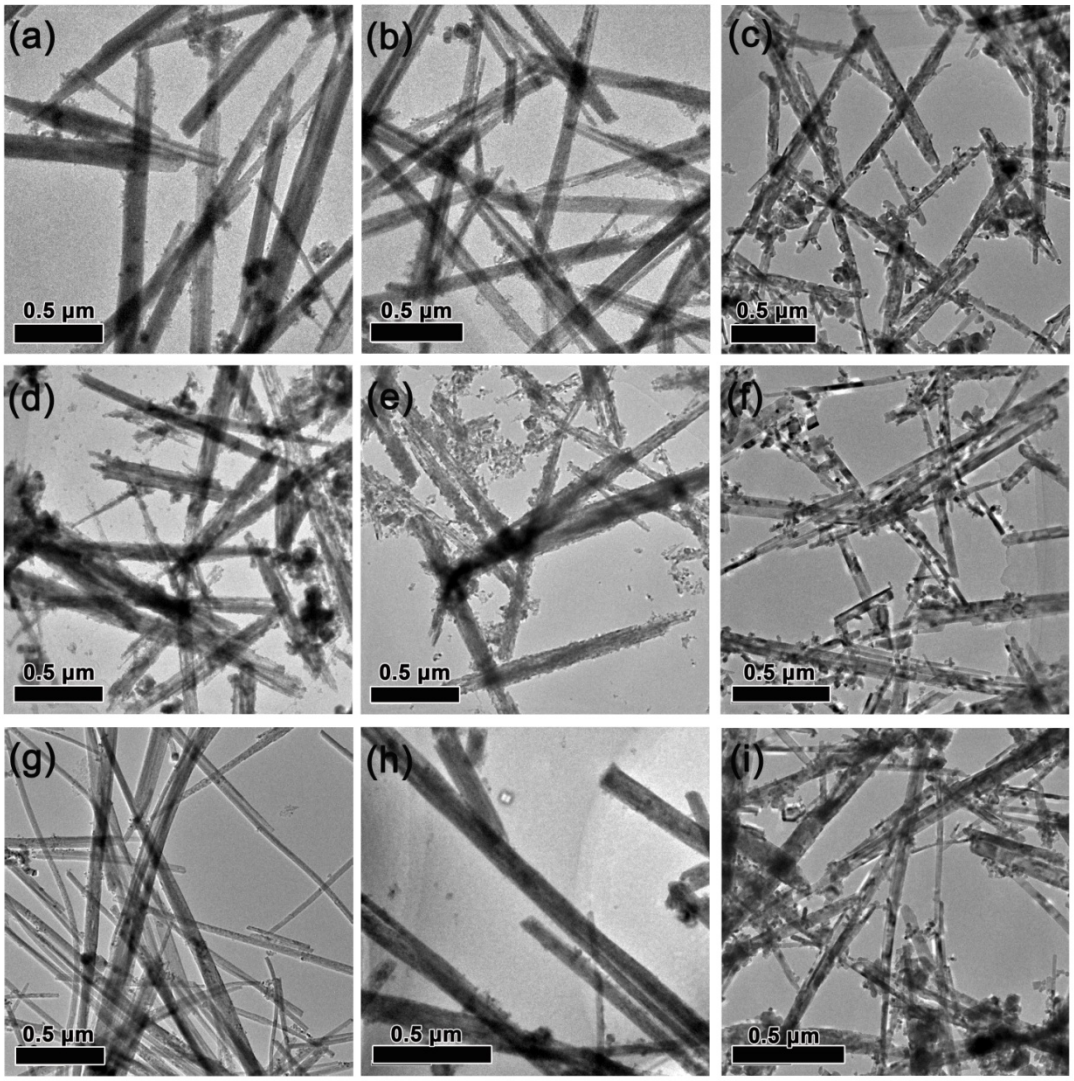

Fig. S3 TEM images of different calcinated products. Images (a) to (i) stand for the samples of Ar-H_2-300, Ar-H_2-500, Ar-H_2-800, Ar-300, Ar-500, Ar-800, Air-300, Air-500 and Air-800, respectively.

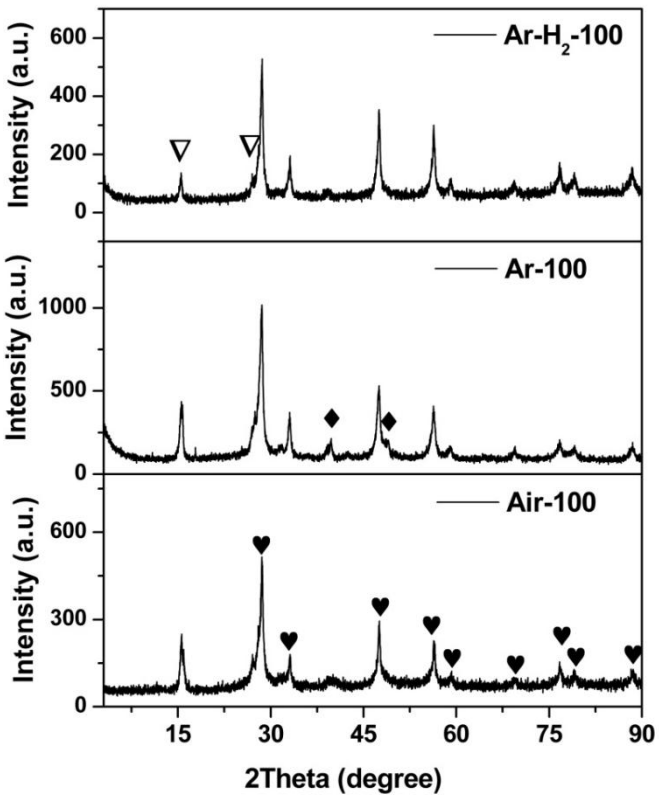

Fig. S4 XRD patterns of products calcinated at 100°C. Symbol ♥, ♦ and ∇ represent the peaks of CeO_2, Ce_2O_3 and $Ce(OH)_3$, respectively.

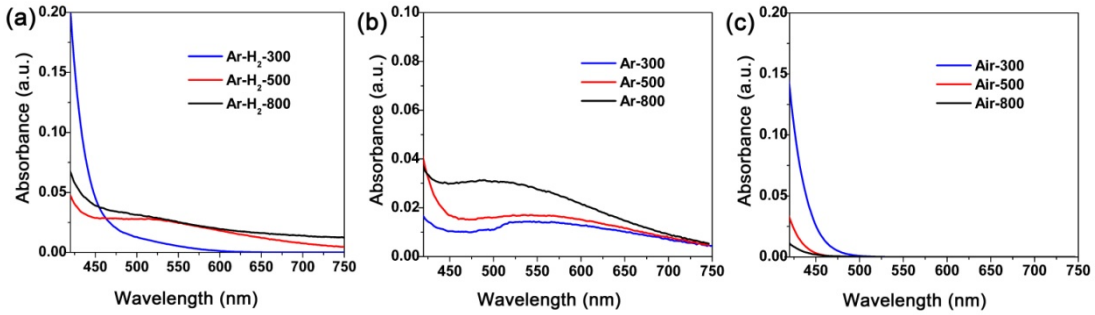

Fig. S5 UV-Vis/DRS spectra of CeO_2 NRs calcinated at 800°C under different atmospheres: (a) Ar-H_2-calcined samples, (b) Ar-calcined samples and (c) Air-calcined samples.

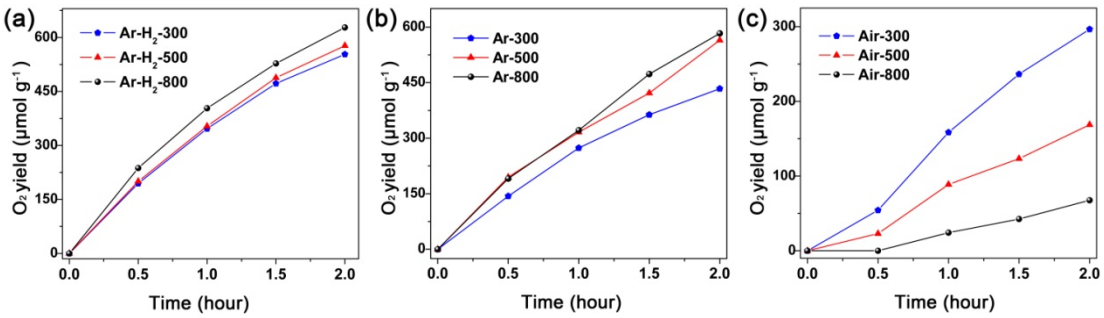

Fig. S6 O_2 evolution as a function of reaction time over different catalysts under visible light irradiation. (a), (b) and (c) stand for Ar-H_2-treated CeO_2 NRs, Ar-treated CeO_2 NRs and Air-treated CeO_2 NRs, respectively. Reaction condition: total water volume, 75 mL; photocatalyst, 50.0 mg; $AgNO_3$, 0.01 M; light source, 300 W Xe lamp, $\lambda \geq 420$ nm.

The photocatalytic performance of different CeO_2 NRs calcinated at different temperatures and atmospheres is evaluated for water oxidation under visible light irradiation ($\lambda \geq 420$ nm). Generally, the products calcinated at 800ºC have the highest catalytic activity except for the sample treated in air.

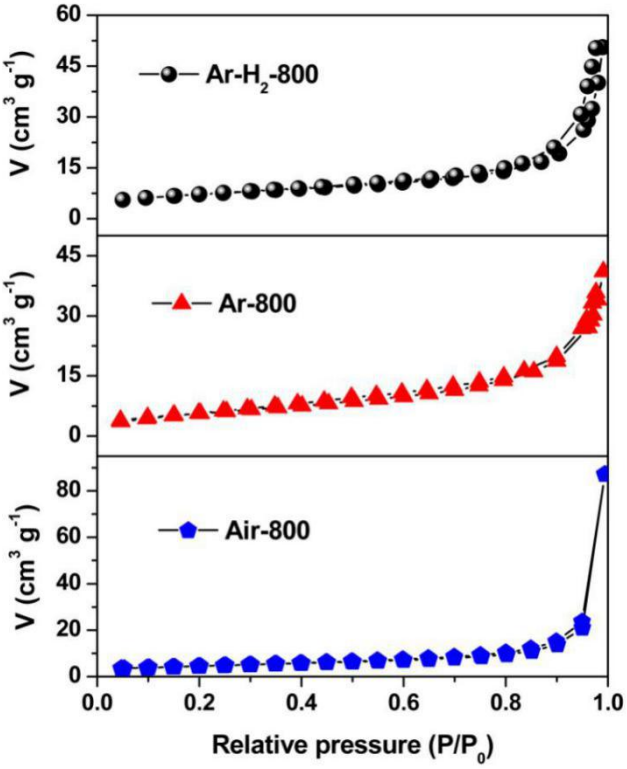

Fig. S7 N_2 adsorption-desorption isotherms of Ar-H_2-800, Ar-800 and Air-800.

As shown in **Fig. S7**, all of the adsorption-desorption isotherms exhibit the type III behaviors, and all the products have similar surface area.

Table S2 Brunauer, Emmett and Teller (BET) surface area of different products.

	300°C ($m^2\ g^{-1}$)	500°C ($m^2\ g^{-1}$)	800°C ($m^2\ g^{-1}$)
Ar-H_2-calcinated	52.98	39.41	25.20
Ar-calcinated	51.28	37.77	20.60
Air-calcinated	50.36	35.42	16.10

The quantitative measurement demonstrates that the products heat-treated at same temperature possess similar surface area regardless of the calcination atmosphere. For example, three samples calcinated at 800ºC have similar BET surface area in the range of 16 $m^2\ g^{-1}$ to 25 $m^2\ g^{-1}$.

Table S3 The ratio of surface active oxygen and Ce^{3+} of Ar-H_2-800, Ar-800 and Air-800 based on XPS analysis in **Fig. 3b** and **3c**.

Catalysts	Ar-H_2-800	Ar-800	Air-800
Ce^{3+}/total Ce	32.59%	29.96%	17.91%
Active oxygen/total oxygen	24.16%	15.51%	2.05%

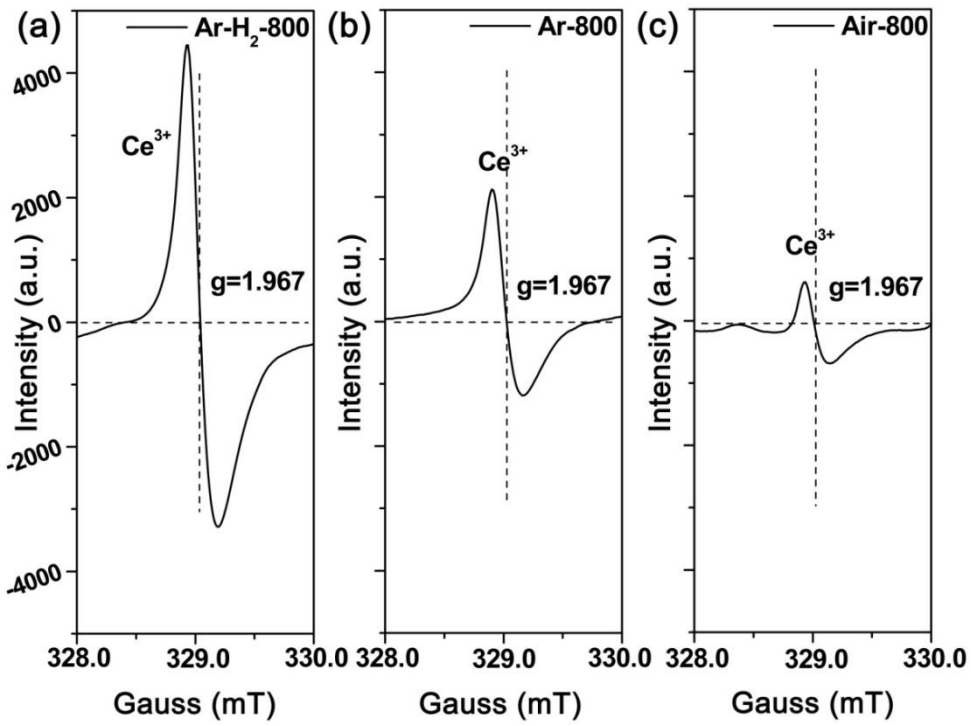

Fig. S8 EPR spectra of Ce^{3+} ions on (a) Ar-H_2-800, (b) Ar-800 and (c) Air-800.

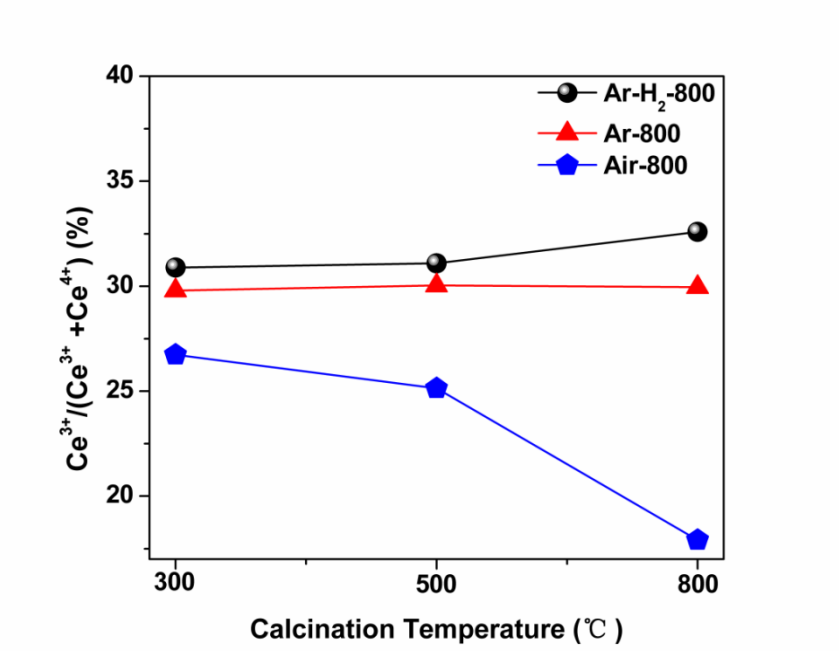

Fig. S9 Surface Ce^{3+} ratio of CeO_2 nanorods heat treated under different conditions. The value is obtained based on Ce 3d XPS analysis.

According to above curves, two conclusions are drawn: (1) At the same calcination temperature, the samples treated under Ar-H_2 have the higher ratio of Ce^{3+} than those under Ar or Air. (2) The samples treated under Ar-H_2 or Ar remain a high ratio of Ce^{3+} regardless of the calcination temperature, but Ce^{3+} ratio of air-calcined samples is decreased remarkably with the increase of calcinations temperature likely due to oxidation of Ce^{3+} by O_2.

Table S4 Initial rate of O_2 generation for three typical catalysts under visible light irradiation.

Catalysts	Ar-H_2-800	Ar-800	Air-800
Initial rate (μmol g^{-1} h^{-1})	474.28 ± 10.89	382.26 ± 10.75	0

Table S5 Photocatalytic property comparison of Ar-H_2-800 with other reported excellent photocatalysts.

Photocatalyst	Light source	Reactant solution	O_2 evolution Activity (μmol h^{-1} g^{-1})	Reference
Ar-H_2-800	Xe lamp, 300 W, $\lambda \geq 420$ nm	$AgNO_3$ 0.01 M	353.87	Our data
Commercial CeO_2	Xe lamp, 300 W, $\lambda \geq 420$ nm	$AgNO_3$ 0.01 M	36.78	Contrast experiment
WO_3	Xe lamp, 300 W, $\lambda \geq 420$ nm	$AgNO_3$ 0.01 M	163.00	*J. Catal*., 2013, **307**, 148-152.
WO_3-H_2-100	Xe lamp, 300 W, $\lambda \geq 420$ nm	$AgNO_3$ 0.01 M	325.50	*J. Catal*., 2013, **307**, 148-152.
WO_3-H_2-200	Xe lamp, 300 W, $\lambda \geq 420$ nm	$AgNO_3$ 0.01 M	376.50	*J. Catal*., 2013, **307**, 148-152.
WO_3-H_2-300	Xe lamp, 300 W, $\lambda \geq 420$ nm	$AgNO_3$ 0.01 M	279.50	*J. Catal*., 2013,**307**, 148-152.
WO_3-H_2-400	Xe lamp, 300 W, $\lambda \geq 420$ nm	$AgNO_3$ 0.01 M	219.50	*J. Catal*., 2013, **307**, 148-152.
WO_3-H_2-500	Xe lamp, 300 W, $\lambda \geq 420$ nm	$AgNO_3$ 0.01 M	0	*J. Catal*., 2013, **307**, 148-152.
Au(1.0 %)/CeO_2	Xe-doped mercury lamp, 220 W, $\lambda \geq 400$ nm	$AgNO_3$ 0.01 M	233.30	*J. Am. Chem. Soc.*, 2011, **133,** 6930-6933.

Graphene-CeO_2	Xe lamp, 150 W,780 nm > λ >250 nm	$AgNO_3$ 0.1 M	125.30	*ACS Catal*., 2014, **4**, 497-504.
Sb/Cr/TiO_2 (rutile)	Xe lamp, 300 W, λ ≥ 420 nm	$AgNO_3$ 0.05 M	63.00	*J. Phys. Chem. B*,2002, **106**, 5029-5034.
Sb/Cu/TiO_2 (rutile)	Xe lamp, 300 W, λ ≥ 420 nm	$AgNO_3$ 0.05 M	11.00	*J. Phys. Chem. B*,2002, **106**, 5029-5034.
Sb/Ni/TiO_2 (rutile)	Xe lamp, 300 W, λ ≥ 420 nm	$AgNO_3$ 0.05 M	25.60	*J. Phys. Chem. B*,2002, **106**, 5029-5034.
Au(1.5 %)/TiO_2	Xe lamp, 300 W, λ ≥ 400 nm	$AgNO_3$ 0.01 M	165.30	*J. Am. Chem. Soc*., 2011, **133**, 595-602.

The performance of photocatalytic water oxidation by the Ar-H_2-800 is further compared with those excellent catalysts reported recently, and the corresponding results summarized in **Table S5**, Impressively, under the similar water oxidation condition, the activity of Ar-H_2-800 outperforms most reported catalysts and the commercial CeO_2 nanoparticles only expect WO_3-H_2-200. Evidently, the Ar-H_2-800 has great potential as a promising photocatalyst for O_2 evolution under visible light irradiation.

Table S6 Control experiments for photocatalysis.

	Pure water	$AgNO_3$ (added or not)	Photocatalyst	Light source (on or off)	Oxygen yield (μmol g^{-1} h^{-1})
Contrast 1	75 mL	0 g	Ar-H_2-800	on	0
Contrast 2	75 mL	0.128 g	No	on	0
Contrast 3	75 mL	0.128 g	Ar-H_2-800	off	0
Contrast 4	75 mL	0.128 g	Ce-based NRs	on	0

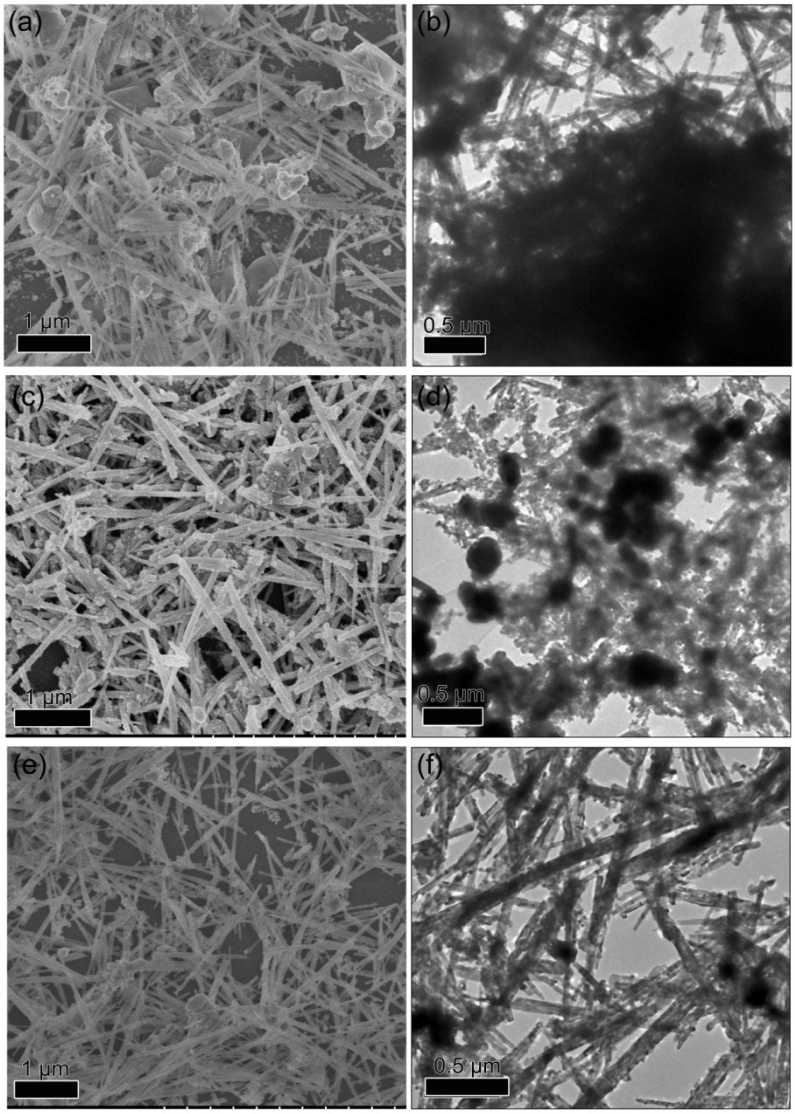

Fig. S10 SEM (a, c, e) and TEM (b, d, f) images after three cycles of water oxidation using (a, b) Ar-H_2-800, (c, d) Ar-800 and (e, f) Air-800, respectively.

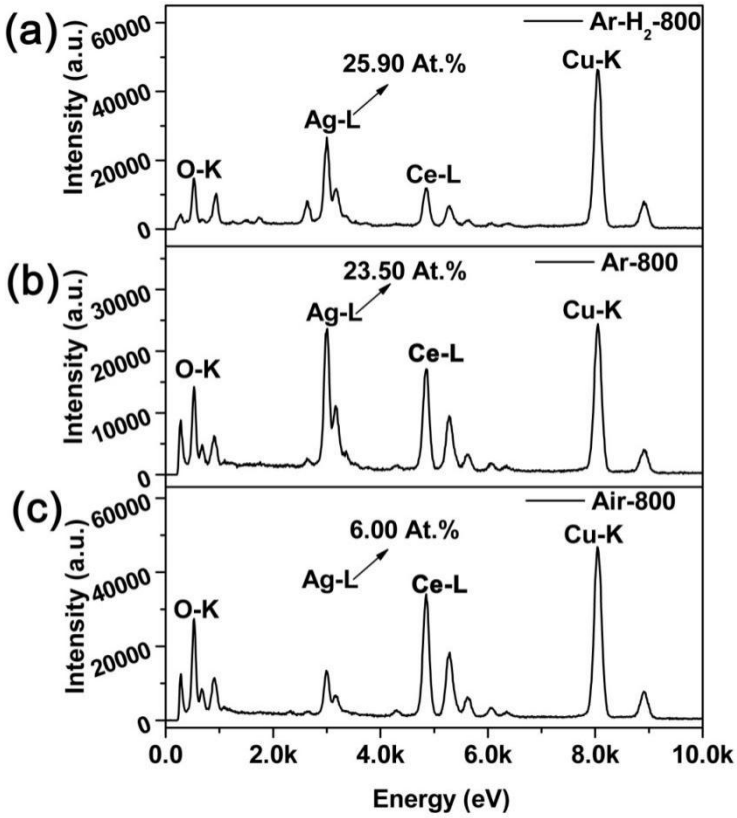

Fig. S11 EDX spectra of the catalysts after three cycles of water oxidation. (a) Ar-H_2-800, (b) Ar-800 and (c) Air-800.

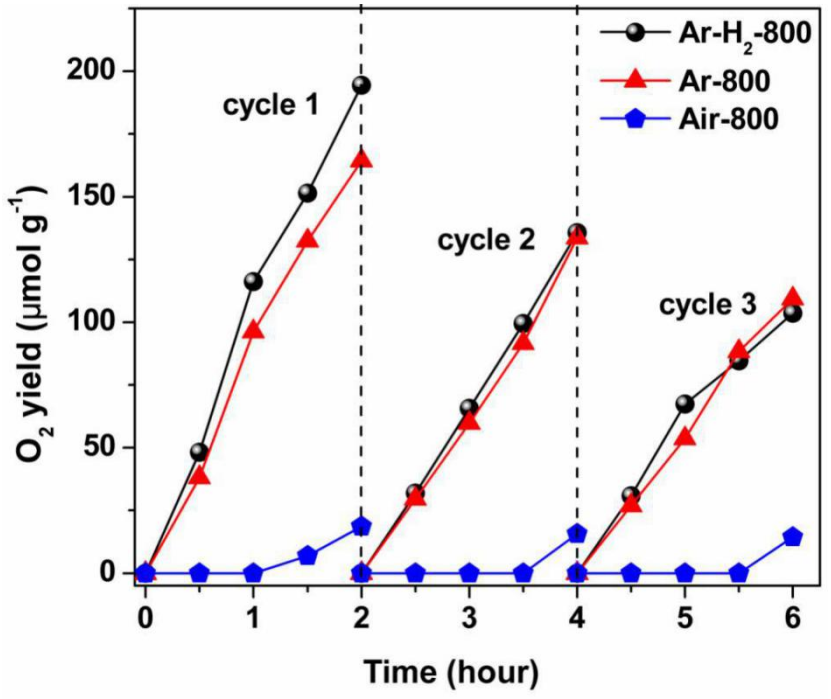

Fig. S12 O_2 evolution of the catalysts by a series of repeated purge and injection cycles with an interval of 2 h. Reaction conditions: total water volume, 75 mL; photocatalyst, 50.0 mg; $Ce(NH_4)_2(NO_3)_6$, 0.01 M; light source, 300 W Xe lamp, $\lambda \geq 420$ nm.

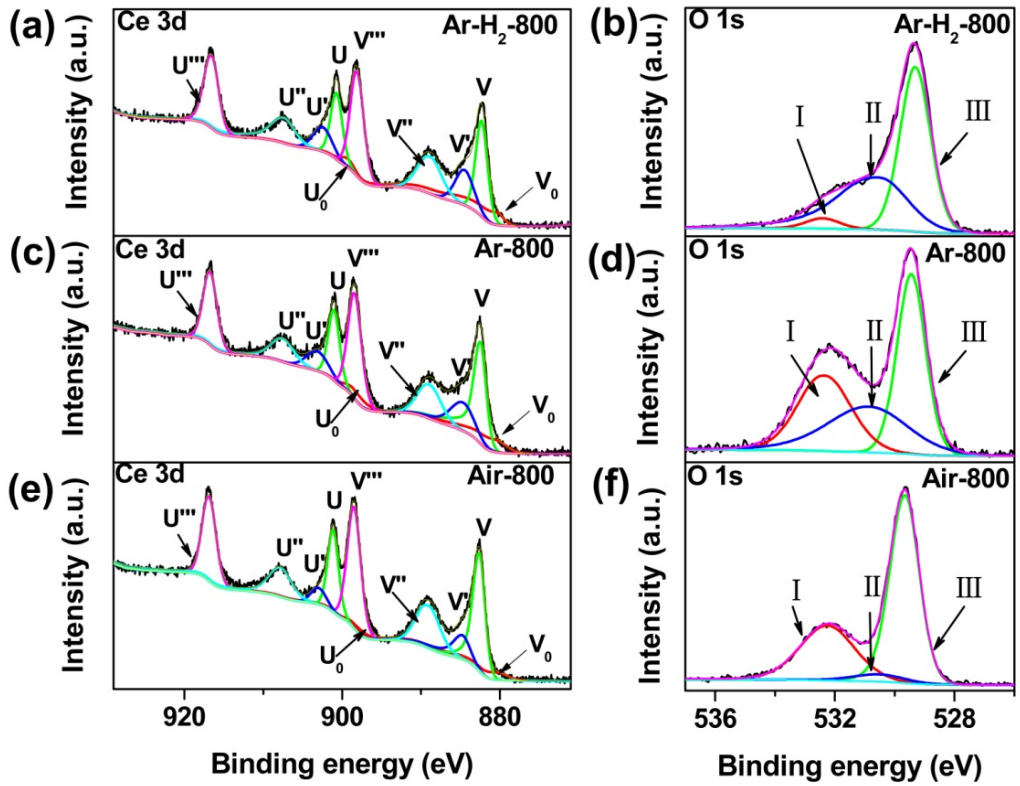

Fig. S13 Ce 3d XPS spectra of (a) Ar-H_2-800, (c) Ar-800 and (e) Air-800 after three cycles of water oxidation. O 1s XPS spectra of (b) Ar-H_2-800, (d) Ar-800 and (f) Air-800 after the three cycles of water oxidation.

U''', V''', U'', V'', U, V, U', V', U_0 and V_0 represent the peaks of Ce^{4+} $3d_{5/2}$, Ce^{4+} $3d_{3/2}$, Ce^{4+} satellite, Ce^{4+} satellite, Ce^{4+} satellite, Ce^{4+} satellite, Ce^{3+} $3d_{5/2}$, Ce^{3+} $3d_{3/2}$, Ce^{3+} satellite and Ce^{3+} satellite, respectively; while I, II and III stand for the peak of absorbed oxygen, active oxygen and lattice oxygen, respectively.

Table S7 The ratio of surface Ce^{3+} and different-typed O after three cycles of water oxidation. The values are obtained based on XPS results (**Fig. S13**).

Catalysts	Ar-H_2-800	Ar-800	Air-800
Absorbed oxygen	8.75%	36.30%	33.74%
Active oxygen	22.43%	18.28%	4.36%
Lattice oxygen	68.82%	44.42%	61.90%
Ce^{3+} / Total Ce	20.55%	22.50%	15.31%

After three cycles of water oxidation, the absorbed oxygen on the catalyst surface is decreased sharply. Especially, the Ar-H_2-800 sample contains the least absorbed oxygen. In addition, the ratio of Ce^{3+} is also decreased with the reaction continuing, indicating that partial Ce^{3+} ions are oxidized into Ce^{4+} ions. It is known that less absorbed oxygen or hydroxyl groups as well as decreased Ce^{3+} ratio would give rise to a decreased photocatalytic activity.

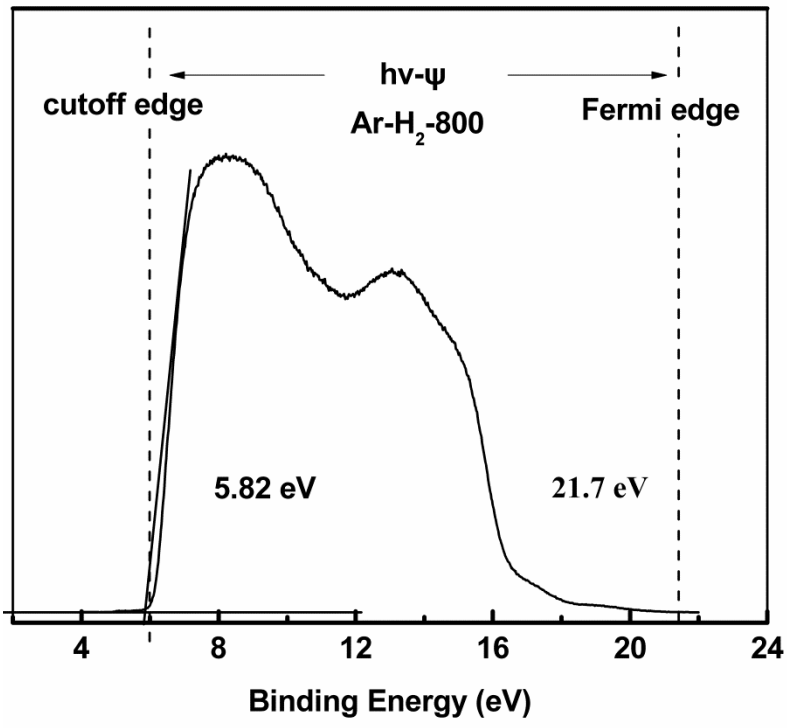

Fig. S14 UPS profiles for Ar-H_2-800 photocatalyst.

Ultraviolet photoelectron spectroscopy (UPS) measurement is used to determine the work function of the CeO_2 samples, which is carried out with Helium Iα as the ultraviolet source. The wavelength of the ultraviolet is 58.13 nm and the kinetic energy (**hυ**) is 21.22 eV. Since all three samples are immobilized on the conducting adhesive, it is reasonable that they have the same Fermi level edge at 21.7 eV (**Fig. S14**). Notably, **Fig. S14** also displays that the binding energy of the cutoff edge for all three samples is 5.82 eV (the intercept of binding energy at the linear area of the UPS curve). Therefore, the work function (**Ψ**) of the CeO_2 samples may be calculated by Eq. (1)**:**

$$\mathbf{\Psi = h\upsilon + E_{cutoff\ edge} - E_{Fermi\ edge}}$$

The work function of all three CeO_2 samples is calculated to be 5.34 eV, so we conclude that the energy difference between Fermi level and vacuum energy of the CeO_2 samples is 5.34 eV (**Scheme 1**).

According to XPS-VB spectra in **Fig. 5**, we know that the energy difference between the Fermi level and the VBM of the CeO_2 samples is about 2.4 eV, thus the energy level of the VBM is located at 7.74 eV (5.34 eV + 2.4 eV). Moreover, since the band gap of Ar-H_2-800 is estimated to

be ~3.24 eV (**Fig.** S15), one can deduce that the energy level of its CBM is set at 4.50 eV (7.74 eV - 3.24 eV). Altogether, we can draw the detailed energy band diagram (**Scheme 1**), and it is obvious that as-synthesized CeO_2 NRs belong to n-type semiconductors.

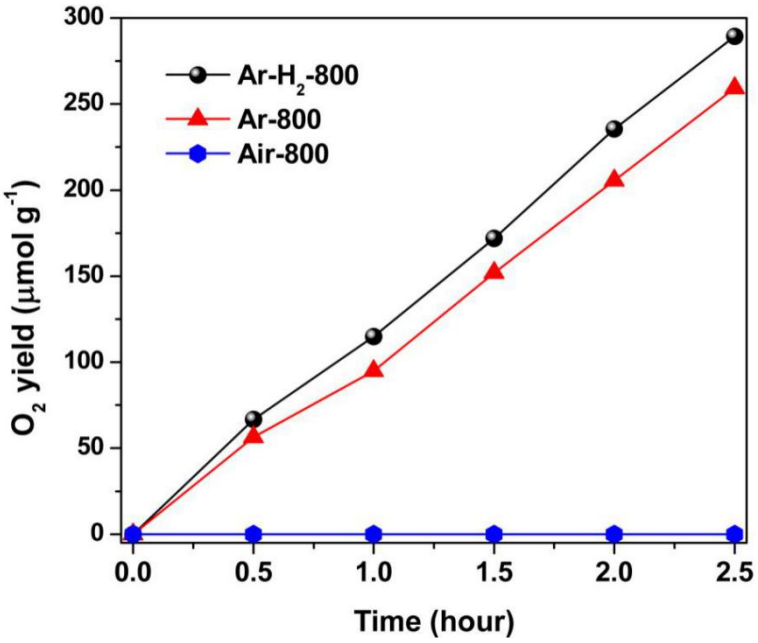

Fig. S15 O_2 evolution of Ar-H_2-800, Ar-800 and Air-800 under visible light irradiation using 500 nm cut filter. Reaction conditions: total water volume, 75 mL; photocatalyst, 50.0 mg; $AgNO_3$ 0.01 M; 300 W Xe lamp, $\lambda \geq 500$ nm.